

Time-resolved pattern evolution in a large-aperture class A laser

I. Leyva*

Nonlinear Dynamics and Chaos Group, Universidad Rey Juan Carlos, 28933 Móstoles, Madrid, Spain

J. M. Guerra†

Departamento de Optica, Facultad de Ciencias Físicas, Universidad Complutense de Madrid, 28040 Madrid, Spain

(Received 15 October 2001; revised manuscript received 23 April 2002; published 28 August 2002)

Quasi-instantaneous transverse patterns have been measured in a broad-aperture class A laser, using an ultrafast camera. The evolution from order to fully developed turbulence is observed as the Fresnel number increases up to 110. In the turbulent regime, two very different spatial scales coexist, one order of magnitude apart. The linear analysis allows us to interpret most of the features of the experiment.

DOI: 10.1103/PhysRevA.66.023820

PACS number(s): 42.65.Sf, 42.55.Mv

I. INTRODUCTION

Large-aperture optical systems are very complex devices having a rich spatiotemporal dynamics. A great deal of experimental work in this field has been carried out with class *B* lasers (in particular CO_2 , [1–4]), and more recently also in semiconductor lasers [5,6]. However, much less research has been devoted to class *A* lasers [7–9], mainly due to their quivalence with slower devices (and, therefore, easier to deal with) as optical parametric oscillator (OPO), degenerate optical parametric oscillator (DOPO), etc. [10–12].

On the theoretical side, a considerable effort has been made to predict, from the basis of the Maxwell-Bloch equations, the spatiotemporal behavior of large-aperture lasers [2,13,14]. Hence, in order to make a comparison with these predictions, it becomes of major interest to measure time-resolved transverse patterns. Unfortunately, so far the extremely fast dynamics of the lasers kept us from obtaining direct evidence of the time-resolved pattern evolution, and only averaged patterns have been reported [1,3,5].

Just recently, our group has obtained experimentally instantaneous snapshots of a broad-aperture CO_2 laser, representative of the class *B* [15,16]. In those works we studied the complete spatiotemporal dynamics of the system, which could be reproduced by means of a model based on the Maxwell-Bloch equations. Following this line, in the present work we study, both experimentally and theoretically, the time-resolved spatial dynamics of a large Fresnel number pulsed dye laser, representative of the class *A*. In particular, instantaneous snapshots of the transverse spatial distribution of the intensity have been measured, showing several important differences with class *B* lasers.

II. EXPERIMENTAL RESULTS

Several works have been carried out previously in our group studying the local dynamics of this dye laser [9,17–21]. From these studies we know that two different spatiotemporal behaviors coexist in the system. First, a turbulent

fast local dynamics with a characteristic period of about 50–100 MHz and a very small spatial correlation length of about 50 μm . In addition, there is a slower dynamics, with periods of more than 100 ns, whose correlation length is of the order of 1 mm. Therefore, it seems that two different levels of spatiotemporal order have to be considered in our system, as have been reported in other broad-aperture class *A* equivalent optical systems [13,22].

This indirect information about the spatiotemporal behavior makes us wonder if the two temporal scales have observable spatial correspondence, as it could be deduced from its correlation lengths [9]. Hence, two experiments have been performed. First, we have obtained quasi-instantaneous measurements of the full pattern with different aperture sizes, to observe the evolution from a moderate to a high Fresnel number. As we will show in detail, we are able to observe the evolution of the turbulence, from a state influenced by the geometrical conditions of both the cavity and the gain, to a state dominated by the inner dynamics of the bulk medium. In the second experiment we enlarge part of the pattern by means of an optical device, in order to uncover the short-correlation length structures whose temporal fast dynamics we had observed previously.

A. Setup

The complete setup used in both experiments is sketched in Fig. 1. Our source is a coaxial flash lamp (FL in Fig. 1) pumped untuned dye laser having a flat-flat resonator (mirrors reflectivities $R_1 = 0.3$ and $R_2 = 0.997$, respectively). The cavity length is $L = 1$ m. A Rhodamine 6G solution in methanol, with a concentration 5×10^{-5} mol/l, was circulated through the flash-lamp inner tube, whose active diameter is 18 mm and overall discharge length was 320 mm. The dye flow velocity is 6 l/min, several order of magnitude slower than the intensity dynamics, as we have observed

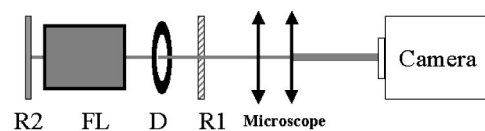


FIG. 1. Experimental setup: **R2**, total reflective mirror. **FL**, coaxial flash lamp. **D**, diaphragm. **R1**, partial reflector mirror.

*Electronic address: ileyva@escet.urjc.es

†Electronic address: jmguerra@fis.ucm.es

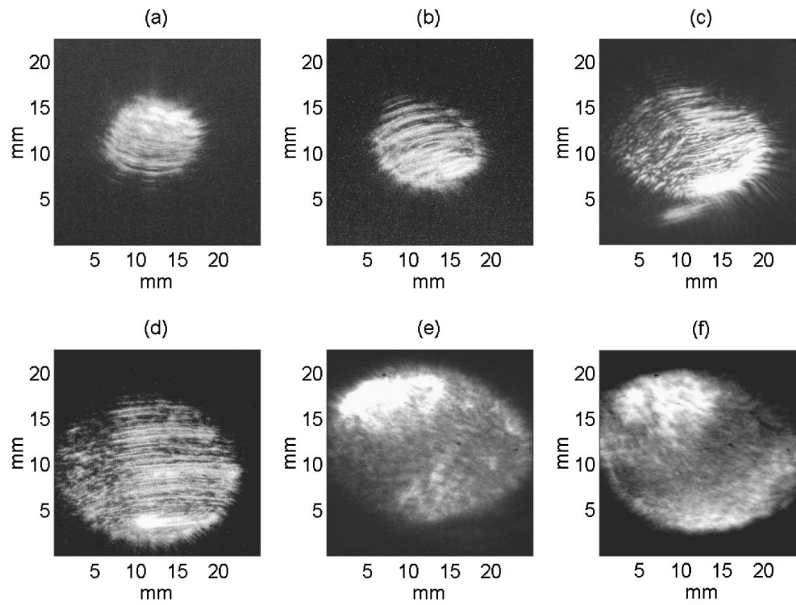


FIG. 2. Instantaneous snapshots of the dye laser transverse pattern, obtained with a 10-ns exposure time and aperture sizes of (a) 6, (b) 8, (c) 9, (d) 12, (e) 14, and (f) 16 mm. Real images size: 20×20 mm.

previously. Therefore, we can consider the dye flow as stationary for all purposes. The laser is operated in a single shot regime leaving enough time between two shots to avoid accumulating radial thermal gradients.

An intracavity diaphragm (**D**) allows us to change continuously the Fresnel number from 10 (diaphragm diameter 6 mm) up to 110 (diaphragm diameter 16 mm). Eventually, we can make the light to go through a broad-aperture telescope without distortion. By means of this device, with a maximum $\times 10$ magnification, it is possible to obtain detailed images of small areas of the spot.

Finally, the light reaches the recording system, which consists of a camera incorporating a fast microchannel plate intensifier with a 750×750 pixel array. The maximum time resolution of 10 ns is fast enough to register the instantaneous evolution of the pattern, and the spatial resolution of $30 \mu\text{m}$ per pixel allows us to resolve the details of the laser spot. The camera shutting system is synchronized with the laser shot.

B. From moderate to high Fresnel number

By means of the intracavity diaphragm **D** (Fig. 1), we perform a systematic reduction of the system aperture, from the maximum possible Fresnel number $\mathcal{F} \approx 106$, down to $\mathcal{F} \approx 15$. For smaller sizes, the gain becomes insufficient to maintain the laser operation and the system falls under threshold, even for the highest excitation that can be reached. In order to have equivalent measurements for each diaphragm, we have taken into account the threshold decrease with the increase of the diaphragm size, so that the measurements were made using an excitation twice over threshold for each diaphragm size.

As it is well known, in an unstable resonator (flat-flat mirrors) as ours, Gaussian modes are not possible. For very small Fresnel numbers, Bessel modes could appear [23,24], but this is not our case since even the smallest aperture we can use is still too large to obtain a simple modal pattern. Instead, from the theory of broad-aperture lasers we know

that positive detuning favors the growth of a traveling transversal wave, which manifests itself as an off-axis emission or tilted wave [25]. The spatial period of this kind of pattern is determined by inner parameters of the laser, but the travel direction of the wave is not theoretically determined. This spatial symmetry breaks due to the nonlinear competition between the different possible waves, or due to anisotropies in the mirror alignment or the gain distribution.

Our observations in this first experiment support the mentioned interpretation, although they show some small deviations from theory due to the fact that a real broad-aperture laser does not satisfy the ideal conditions, such as infinite transverse size or spatially homogeneous gain. In Fig. 2 we show different results of snapshots obtained with a 10-ns exposure and aperture sizes of 6, 8, 9, 12, 14, and 16 mm, respectively. The images have been treated to increase the contrast, in order to appreciate the details.

We observe that for $\mathcal{F} \approx 15$ [Fig. 2(a)], the laser presents a striped pattern corresponding to the intensity of a tilted wave, with a spatial period of about 0.5 mm. The tilting of the stripes, which varies slightly from shot to shot, is due to the symmetry breaking caused by the small anisotropies, as was mentioned above. Therefore, in this regime, in which the total available energy is not very high, the pattern geometry seems to be strongly influenced by inner anisotropies or misalignments. However, as expected, the pattern does not retain the circular geometry of the boundary condition. Vortices or defects are not observed in any case.

As \mathcal{F} increases, [Figs. 2(b)-2(d)], the stripes do not extend from side to side of the aperture, but they break in smaller structures. However, the mean transversal structure size is still about 0.5 mm, not showing measurable dependences with the aperture, as could be deduced from the theoretical prediction. Finally, for even bigger Fresnel numbers [Figs. 2(e) and 2(f)], the stripes almost disappear yielding to a granular intensity distribution, without a preferred direction. Nevertheless, in Fig. 2(f) small stripe domains, with different tilting, can be observed.

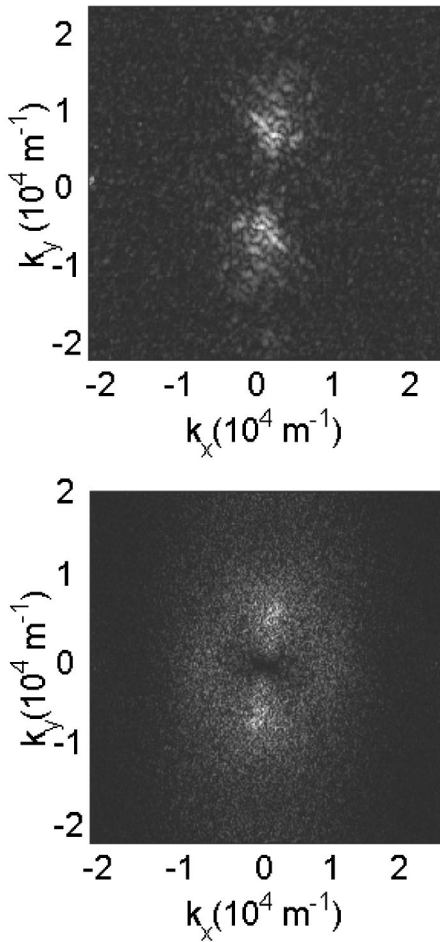


FIG. 3. Spatial power spectra of the transverse intensity snapshots for the aperture sizes of (a) 6 mm (b) 16 mm.

Therefore, it appears that, as the effective transversal size is larger, the anisotropy of the gain medium losses influence on the selection of the pattern, allowing the survival of different waves with the same wavelength but traveling in different directions [26].

The structures in the instantaneous photographs are complex and their average structures size is difficult to determine. Therefore, we perform the spatial power spectra in order to observe in the Fourier plane the characteristic size and direction. In Fig. 3 are shown the spatial power spectra of the instantaneous intensity distribution when the aperture system is 6 mm [Fig. 3(a)] and 16 mm [Fig. 3(b)], respectively. It is observed that in the small-aperture case the preferred direction is very strongly determined, whereas for big aperture sizes the ring-shaped power spectrum indicates the existence of spatial frequency contributions in all directions, due to the loss of influence of cavity anisotropies.

However, the absolute dominant spatial frequency does not vary significantly. It can be observed that the maximum contribution corresponds to a transverse wave number $k_o \approx 7000 \text{ m}^{-1}$, which is equivalent to an approximate structure size of $S_o = 450 \text{ }\mu\text{m}$, as it was estimated from the photographs.

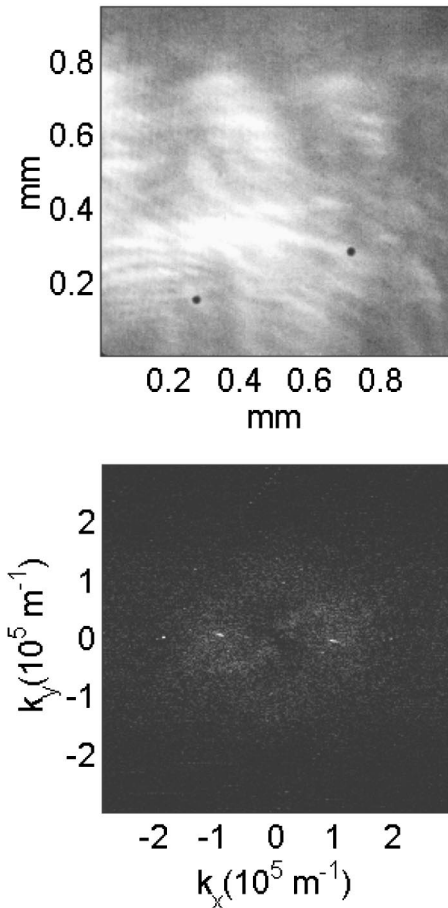


FIG. 4. (a) Detail of an instantaneous snapshot of the amplified transverse pattern. Real size of the amplified area in the photography: 1 mm \times 1 mm, (b) spatial power spectrum of (a).

To be sure that the observed structures are due to the system dynamics, and not due to other effects such as inhomogeneities in the turbulent liquid host, we have repeated the experiment without any flux. The results are the same, therefore we can discard this possibility.

Hence, in this experiment it is observed the instantaneous dynamics of the transverse traveling wave. It is observed an evolution from a relatively ordered situation when the Fresnel number is $\mathcal{F} \approx 15$ [Fig. 2(a)], to a well developed turbulence when $\mathcal{F} > 100$ [Fig. 2(f)].

C. Structure coexistence

Once we have observed the big-scale structure in the pattern, we look for the small structure from which we have indirect evidence. In order to perform this measurement, we place after the laser output a broad-aperture telescope that allows us to magnify the image up to 10 times the original size. Therefore, the spatial resolution of the system increase to 3 μm , but for this experiment just 256×256 pixels are active.

An example of these measurements is shown in Fig. 4(a). The instantaneous image, taken with a 10-ns exposure, corresponds to a real area of around $1 \times 1 \text{ mm}^2$ in the pattern without amplification. We find that each big structure ob-

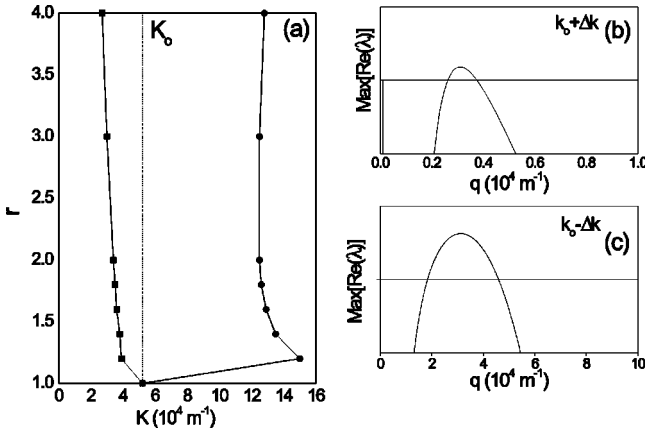


FIG. 5. Results of the stability analysis of the Maxwell-Bloch model: (a) Neutral stability curves when $\delta=0.02$, around the critical wave $k_o=5 \times 10^4$ m. Maximum value of the real parts of the complete Maxwell-Bloch model eigenvalues for $r=2.0$ and: (b) $k > k_o$, (c) $k < k_o$.

served in the measurements without magnification consists of a cluster of smaller structures. As it was made for the full pattern, we perform the corresponding power spectrum in order to measure this structure size. As can be seen in Fig. 4(b), the maximum contribution in the spectrum corresponds to a spatial frequency of $k_o=5 \times 10^4$ m⁻¹, equivalent to a spatial period of $S_o=60$ μm.

Therefore, we conclude that in this system actually coexist spatiotemporal structures with two different spatial scales, one order of magnitude apart.

III. MODEL AND THEORETICAL RESULTS

In the dye laser, the gain line is $\delta\nu \sim \gamma_{\perp} \approx 1$ THz wide, and the free spectral range is $c/2L = 150$ MHz. Therefore the number of longitudinal modes that may be active is ~ 6600 . However, it is possible to consider every longitudinal mode as independent, all of them behaving in an equivalent way. In consequence, we will obtain information about the spatiotemporal dynamics of our system from the Maxwell-Bloch (MB) monomode model [2,15]:

$$\frac{\partial E}{\partial t} = -\kappa \left[1 - i\delta - \frac{ia}{2} \Delta_{\perp} \right] E - \kappa r P, \quad (1)$$

$$\frac{\partial P}{\partial t} = -\gamma_{\perp} [(1 + i\delta)P + ED],$$

$$\frac{\partial D}{\partial t} = -\gamma_{\parallel} \left[D - 1 - \frac{1}{2}(E^*P + EP^*) \right],$$

where $E=E(\mathbf{x},t)$ is the slowly varying electric field, $P=P(\mathbf{x},t)$ the polarization, $D=D(\mathbf{x},t)$ the population inversion, $r=r(\mathbf{x},t)$ the rescaled pump. The κ parameter represents the cavity losses, $a=c\lambda/2\pi\kappa$ is a diffraction coefficient and $\delta=(\omega_{21}-\omega)/(\gamma_{\perp}+\kappa)$ the rescaled detuning, where ω_{21} is the frequency of the transition, ω is the fre-

quency of the laser emission, and c is the speed of light. In addition, Δ_{\perp} is the Laplacian in the transverse coordinates of the system, $\mathbf{x}=(x,y)$. In dye lasers, the polarization decay rate is as $\gamma_{\perp} \approx 10^{12}$ s⁻¹ and the inversion decay rate as $\gamma_{\parallel} \approx 4 \times 10^8$ s⁻¹. The losses coefficient will be taken as $\kappa = c \ln(R)/4L = 1.5 \times 10^8$ s⁻¹, where $L=1$ m.

In order to understand the origin of the spatial frequencies observed in the system, we center our theoretical study in the linear stability analysis. This is a powerful tool that has been extensively used [2,25,27]. To our knowledge, these analysis have been applied only to class B or C lasers, and have not been particularized for class A lasers. In addition, as far as we know, the conclusions coming from the analysis have not been but occasionally contrasted with real broad-aperture lasers [5,16].

As it is well known, the stability of the nonlasing solution $E=P=0$, $D=1$ yields the following neutral stability threshold:

$$r(k) = 1 + \left(\frac{\delta(\gamma_{\perp} + \kappa) - \frac{a}{2} \kappa k^2}{\gamma_{\perp} + \kappa} \right)^2, \quad (2)$$

where k is the transverse wave number of the corresponding traveling wave. The transverse wave number with the lower threshold is called the critical wave

$$k_o = \sqrt{\frac{2\delta(\gamma_{\perp} + \kappa)}{a\kappa}}. \quad (3)$$

However, being our system a multimode one, the detuning parameter δ is not well defined. Nevertheless, we can estimate an effective δ value by considering which detuning value is needed to obtain a stationary transverse wave having the spatial frequency k observed in the measurements. Thus, we will use the main spatial frequency observed experimentally for the small size structures, $k_o = \pi/S_{exp} \approx 5 \times 10^4$ m⁻¹, as the ansatz critical wave. Substituting the dye laser parameters in Eq. (3), we obtain an effective detuning value of $\delta \approx 0.02$. We will use this value in all our posterior calculations. This is the most energetically favored solution immediately after threshold. When the pump increases, new solutions k are allowed in the system. But also these initially allowed k lasing solution can be themselves destabilized and damped, yielding their energy the other new structures raising in the system, more energetically favored for the new pump value. Therefore, to obtain information about our system behavior for other r values, we need to study the stability of the primary traveling wave solutions k perturbed by secondary solutions in the form of traveling-waves of wave vector \mathbf{q} [16,28]. Hence, we linearize the Maxwell-Bloch equations around an arbitrary traveling solution with homogeneous amplitude, $E_t = E_{ot} e^{i(\mathbf{kx} - \omega t)}$, $P_t = P_{ot} e^{i(\mathbf{kx} - \omega t)}$, and $D_t = D_{ot}$, where \mathbf{k} is the wave vector of a traveling solution arising from the unstabilization of the nonlasing solution. Writing the complex fields in the polar form, $E = |E_t| e^{i\Phi E}$, $P = |P_t| e^{i\Phi P}$, it is useful to define the vector variable,

$$U = \begin{pmatrix} E \\ \overline{|E_t|} \\ \Phi_E \\ P \\ \overline{|P_t|} \\ \Phi_P \\ D \\ \overline{|D_t|} \end{pmatrix}. \quad (4)$$

Then, we expand $\mathbf{U} = \mathbf{U}_t + \mathbf{U}_1 e^{i\mathbf{q}\mathbf{x}}$, where \mathbf{U}_t is the solution to be perturbed, and $\mathbf{U}_1(\mathbf{q}, t) e^{i\mathbf{q}\mathbf{x}}$ is a small perturbation. We introduce \mathbf{U} in the MB system, to obtain a linear equation $\partial_t \mathbf{U}_1 = \mathcal{L}_q \mathbf{U}_1$. As the matrix \mathcal{L}_q is time independent, then $\mathbf{U}_1 = \mathbf{u}_q e^{\lambda(q)t}$, where $\lambda(q)$ are Liapunov exponents, i.e., the eigenvalues of the matrix \mathcal{L}_q [13]:

$$\mathcal{L}_q = \begin{pmatrix} -\kappa & -\kappa \left(\delta' - \frac{a}{2} (q^2 + 2kq \cos \alpha) \right) & \kappa & \kappa \delta' & 0 \\ -\kappa \left(\delta' - \frac{a}{2} (q^2 + 2kq \cos \alpha) \right) & -\kappa & -\kappa \delta' & \kappa & 0 \\ \gamma_{\perp} & -\gamma_{\perp} \delta' & -\gamma_{\perp} & \gamma_{\perp} \delta' & \gamma_{\perp} \\ \gamma_{\perp} \delta' & \gamma_{\perp} & -\gamma_{\perp} \delta' & -\gamma_{\perp} & \gamma_{\perp} \delta' \\ -\gamma_{\parallel} \frac{|E_o|^2}{1 + \delta'^2} & \gamma_{\parallel} \frac{|E_o|^2}{1 + \delta'^2} \delta' & -\gamma_{\parallel} \frac{|E_o|^2}{1 + \delta'^2} & -\gamma_{\parallel} \frac{|E_o|^2}{1 + \delta'^2} \delta' & -\gamma_{\parallel} \end{pmatrix}, \quad (5)$$

where $\delta' = \delta + (\omega/\gamma_{\perp})$, and $\omega = a\kappa\gamma_{\perp}/2(\kappa + \gamma_{\perp})k^2$ is the oscillation frequency of the traveling solution \mathbf{k} whose stability is being tested, and α is the angle between this traveling vector \mathbf{k} and the perturbation \mathbf{q} .

The results are shown in Fig. 5, for pump values from threshold $r=1$ up to $r=4$, for wave numbers around the critical wave k_o , and the detuning value δ estimated from the experiment. In the case presented in Fig. 5, the perturbation \mathbf{q} is chosen parallel to the perturbed wave \mathbf{k} , but the results for orthogonal waves are similar.

In Fig. 5(a) we show the neutral stability curves, that is, the pairs (k, r) for which $\max[\text{Re}(\lambda)] = 0$. These represent the boundary between stable k values (inside the lines) and unstable k (outside the lines), for each pump value, r . It can be seen that, as usual, the critical wave remains stable for any r and q values. This means that the system always presents structures whose size can be related to the small scale observed in the photographs. However, the stability is limited both for $k < k_o$ and $k > k_o$ by two asymmetric amplitude instabilities. In order to show how these instabilities manifest themselves in the generation of new wavelengths in the system, in Figs. 5(b) and 5(c) we plot the maximum of the real parts of the system eigenvectors [16], when the pump is $r=2$ as in the experimental system. It can be seen that for wave number larger than k_o [Fig. 5(b)], the instability gives rise to a band of new wavenumbers centered around $q \approx 3$

$q \approx 3 \times 10^3 \text{ m}^{-1}$, which spatially means the appearance of structures with an average size of about 1 mm. Simultaneously, for wave numbers shorter than k_o [Fig. 5(c)], the corresponding instability gives rise to the growing of new traveling waves in a band centered around $q \approx 3 \times 10^4 \text{ m}^{-1}$. That is, in this case the damping of the unstable k waves generates secondary q waves nearer the more favorable k_o .

However, we found a caveat of this simple interpretation of the observed spatial scales when we calculate the corresponding oscillation frequencies, since the frequency associated to the instabilities is of the order of $\omega = 10 \text{ GHz}$, several orders of magnitude higher than the observed ones, about 50–100 MHz. We are aware that our measurement system would not be able of detect such an extremely fast frequency. A possible explanation of this effect from a completely different point of view has been attempted in Refs. [29,30], in which the spatial dynamics was not considered.

IV. CONCLUSIONS

In this work we report the measurements of quasi-instantaneous patterns of a large-aperture class A laser. These photographs reveal the simultaneous presence of two levels of spatial structures, with sizes one magnitude order apart.

The analysis of stability based on the Maxwell-Bloch model shows that, for our experimental conditions, there are two instabilities active having spatial periods of 50 μm and 1 mm, respectively, in good agreement with the observed structures.

ACKNOWLEDGMENT

The authors wish to acknowledge the comments and suggestions of J. R. Pelaez, who has contributed determinantly to the improvement of this work.

-
- [1] D. Dangoisse, D. Hennequin, C. Lepers, E. Louvergneaux, and P. Glorieux, *Phys. Rev. A* **46**, 5955 (1992).
 - [2] G. Huyet, M.C. Martinoni, J.R. Tredicce, and S. Rica, *Phys. Rev. Lett.* **75**, 4027 (1995).
 - [3] G. Huyet and J. Tredicce, *Physica D* **96**, 209 (1996).
 - [4] A. Labate, M. Ciofini, R. Meucci, S. Boccaletti, and F. Arecchi, *Phys. Rev. A* **56**, 2237 (1997).
 - [5] S.P. Hegarty, G. Huyet, J.G. McInerney, and K.D. Choquette, *Phys. Rev. Lett.* **82**, 1434 (1999).
 - [6] O. Hess, S. Koch, and J.V. Moloney, *IEEE J. Quantum Electron.* **31**, 35 (1995).
 - [7] S.G. Chuartzman, D. Krygier, and A.A. Hnilo, *Opt. Commun.* **121**, 1 (1995).
 - [8] D.M. Fondevilla and A.A. Hnilo, *Opt. Commun.* **162**, 324 (1999).
 - [9] V.M. Pérez-García, I. Pastor, and J.M. Guerra, *Phys. Rev. A* **52**, 2392 (1995).
 - [10] K. Staliunas, G. Sleky, and C.O. Weiss, *Phys. Rev. Lett.* **79**, 2658 (1997).
 - [11] C.O. Weiss, M. Vaupel, K. Staliunas, G. Sleky, and V. Taranenko, *Appl. Phys. B: Lasers Opt.* **B68**, 151 (1999).
 - [12] M. Vaupel, K. Staliunas, and C.O. Weiss, *Phys. Rev. A* **54**, 880 (1996).
 - [13] G. Huyet and S. Rica, *Physica D* **96**, 215 (1996).
 - [14] K. Staliunas and C.O. Weiss, *Physica D* **81**, 79 (1995).
 - [15] F. Encinas-Sanz, I. Leyva, and J. Guerra, *Phys. Rev. Lett.* **84**, 883 (2000).
 - [16] F. Encinas-Sanz, I. Leyva, and J. Guerra, *Phys. Rev. A* **62**, 043821 (2000).
 - [17] I. Pastor, F. Encinas-Sanz, and J.M. Guerra, *Appl. Phys. B: Photophys. Laser Chem.* **B52**, 184 (1991).
 - [18] V.M. Pérez-García and J.M. Guerra, *Phys. Rev. A* **50**, 1646 (1994).
 - [19] O.G. Calderón, I. Leyva, and J.M. Guerra, *Appl. Phys. Lett.* **73**, 557 (1998).
 - [20] O.G. Calderón, I. Leyva, and J.M. Guerra, *IEEE J. Quantum Electron.* **35**, 1 (1999).
 - [21] I. Leyva and J. Guerra, *Appl. Phys. Lett.* **77**, 1599 (2000).
 - [22] J. Farjas, D. Hennequin, D. Dangoisse, and P. Glorieux, *Phys. Rev. A* **57**, 580 (1994).
 - [23] A.E. Siegman, *Lasers* (Oxford University Press, Walton Street, Oxford, 1986).
 - [24] O.G. Calderón, V.M. Pérez-García, I. Martín, and J.M. Guerra, *Phys. Rev. A* **53**, 3490 (1996).
 - [25] P. Jakobsen, J. Lega, Q. Feng, M. Staley, J.V. Moloney, and A.C. Newell, *Phys. Rev. A* **49**, 4189 (1994).
 - [26] G. K. Harkness, W. J. Firth, J. B. Geddes, J. V. Moloney, and E. M. Wright, *Phys. Rev. A* **50**, 4310 (1994).
 - [27] J. Lega, J. Moloney, and A. Newell, *Physica D* **83**, 478 (1995).
 - [28] P. Jakobsen, J. Moloney, A. Newell, and R. Indik, *Phys. Rev. A* **45**, 8129 (1992).
 - [29] O.G. Calderón, I. Leyva, and J.M. Guerra, *Appl. Phys. Lett.* **73**, 557 (1998).
 - [30] I. Leyva and J.M. Guerra, *Appl. Phys. Lett.* **77**, 1599 (2000).